Aalto University

OPEN ACCESS

This is an electronic reprint of the original article.
This reprint may differ from the original in pagination and typographic detail.

Leng, Ruoxuan; Li, Zhengmao; Xu, Yan

Joint Planning of Utility-Owned Distributed Energy Resources in an Unbalanced Active Distribution Network Considering Asset Health Degradation

Published in:
IEEE Transactions on Smart Grids

DOI:
10.1109/TSG.2024.3365974

Published: 01/07/2024

Document Version
Peer-reviewed accepted author manuscript, also known as Final accepted manuscript or Post-print

Please cite the original version:
Leng, R., Li, Z., & Xu, Y. (2024). Joint Planning of Utility-Owned Distributed Energy Resources in an Unbalanced Active Distribution Network Considering Asset Health Degradation. *IEEE Transactions on Smart Grids*, *15*(4), 3768-3781. Article 10436425. https://doi.org/10.1109/TSG.2024.3365974

This material is protected by copyright and other intellectual property rights, and duplication or sale of all or part of any of the repository collections is not permitted, except that material may be duplicated by you for your research use or educational purposes in electronic or print form. You must obtain permission for any other use. Electronic or print copies may not be offered, whether for sale or otherwise to anyone who is not an authorised user.

Joint Planning of Utility-Owned Distributed Energy Resources in an Unbalanced Active Distribution Network Considering Asset Health Degradation

Ruoxuan Leng, *Student Member, IEEE*, Zhengmao Li, and Yan Xu, *Senior Member, IEEE*

***Abstract*- Rapid integration of distributed energy resources (DERs) in active distribution networks (ADNs) necessitates advanced planning methods to optimally determine the size, site, and installation time of DERs. However, existing approaches often assume balanced networks and neglect health degradation of DER assets, limiting the accuracy and practicality of the planning results. This paper proposes a new planning method for utility-owned distributed generators (DGs) and energy storage systems (ESSs) in an unbalanced ADN considering asset health degradation. First, the three-phase branch flow is modeled for unbalanced characteristics of ADNs, and host DERs separately in different phases. Then, based on the Wiener degradation process, the aging path of each DG unit is modeled to estimate its available capacity along with service time; the ESS aging is modeled to reflect the degradation cost during charging and discharging. Finally, a copula-based stochastic programming method is presented considering the correlations between renewables and power demands. The inclusion of market volatility in electricity price uncertainty further enhances planning realism. Numerical case studies on an IEEE-34 bus three-phase ADN demonstrate the effectiveness and advantages of the proposed method.**

***Index Terms*—Unbalanced active distribution network (ADN), stochastic programming, correlated uncertainties, degradation.**

NOMENCLATURE

Abbreviations

DE	Diesel generator
DER	Distributed energy resource
DG	Distributed generator
ESS	Energy storage system
RES	Renewable energy resource
PV	Solar photovoltaics
WT	Wind turbine

Sets and Indices

$br/i/p$	Index for branches/buses/phases (a,b,c)
y/m	Index of years/first year of plan phase
$q/d/t$	Index of DG type /day/dispatch period
N_p/N_i	Number of phases/candidate buses
$N_y/N_d/N_t$	Number of years/days/dispatch periods
N_{WT}/N_{DE}	Set of candidate bus for WT/DE
N_{PV}/N_{ESS}	Set of candidate bus for PV/ESS
N_y^{INV}	Set of years which can install new DER

Parameters

λ	Drift parameter denoting the aging rate
$\sigma_B/B(t)$	The standard deviation for degradation volatility / standard Brownian motion
$Y\sim N(0,1)$	Randomness parameters satisfied the normal distribution
$\lambda_{cap}^q/\lambda_{om}^q$	Aging rate of different types of DG
$\sigma_{cap}^q/\sigma_{om}^q$	The standard deviation for degradation volatility of different types of DG
$\Gamma_{cap}^{q,y}/\chi_{om}^{q,y,d,t}$	Capacity-drop level /unit maintenance cost of different types of DG
$E_{ESS}^{p,i,R}$	Rated battery storage capacity
$\varsigma_R^{p,y,i}/L_{ESS}^{p,i,R}$	Rated charge life/life cycle of battery
$DoD_R^{p,i}$	Rated depth of discharge of battery ESS
σ	Discount rate
$\xi_{ESS}^{inv}/\xi_{DG}^{inv}$	Unit investment cost of ESS/DG
γ_{SAL}^y	Salvage value to investment cost ratio
ξ_{DL}^t	Power retail price to local customers
P_{LD}/Q_{LD}	Active /reactive power demands
ξ_{sub}^{RES}	Unit subsidy price for RES
ξ_{pur}^t/ξ_{sell}^t	Power purchasing /selling price
$\chi_{om,ESS}$	Maintenance cost of ESS
$\xi_{em}^{DE}/\xi_{em}^{pur}$	Emission conversion from DE and grid
$C_{ESS_{age}}^{p,y,d,t,i}$	Battery energy storage degradation cost
$\xi_{cur}^{WT}/\xi_{cur}^{PV}$	WT/PV power curtailment cost
$P_{WT,real}/P_{PV,real}$	Available energy resources from WT/PV
$C_{DE}^{up}/C_{DE}^{down}$	Start-up/shut-down cost of DE
$IC_{DG}^{q,unit}$	The unit capacity of different types of DG
$IC_{DG}^{q,MIN/MAX}$	Min/max capacity DG can be installed for each candidate bus
$IC_{DG,ALL}^{p,q}$	Total allowed capacity DG can install
$IC_{ESS}^{MIN/MAX}$	Min/max capacity ESS can be installed for each candidate bus
$IC_{ESS,ALL}^{p}$	The total allowed capacity ESS can install
β_{LL}	Leakage loss ratio of ESS
$\beta_{de}^{min}/\beta_{de}^{max}$	Min/max power output rate of DE
$R_{DE}^{up}/R_{DE}^{down}$	Ramping up/down rates of DE
$\beta_{esc}^{min}/\beta_{esc}^{max}$	Min/max allowed charging power
$\beta_{esd}^{min}/\beta_{esd}^{max}$	Min/max allowed discharging power
$\gamma_{ess}^{min}/\gamma_{ess}^{max}$	Min/max state of charge
$\tau_{es}/\eta_{esc}/\eta_{esd}$	ESS Decay rate/charging or discharging efficiency of ESS
S_{TF}^{max}	Max transformer power limit
V_{min}^2/V_{max}^2	Min/max voltage square limits

R. Leng, Z. Li and Y. Xu, are with Nanyang Technological University, Singapore (E-mail: ruoxuan002@e.ntu.edu.sg, lizh0049@e.ntu.edu.sg, eeyanxu@gmail.com). The work in this paper is supported in part by SP Group-NTU Joint Lab under Project #1)

Variables

$X(t)$	DG degradation level at time *t*
$C_{INV}^{y}/C_{SAL}^{N_y}$	Investment cost/salvage cost
C_{rev}^{y}/C_{sub}^{y}	Revenue from customers / RES subsidy
C_{ex}^{y}/C_{om}^{y}	Power transaction/maintenance cost
C_{em}^{y}/C_{age}^{y}	Gas emission/battery degradation cost
C_{st}^{y}/C_{sd}^{y}	Start-up/shut-down cost
C_{curt}^{y}	RES curtailment cost
$IC_{DG}^{p,q,y,i}$	The new installed capacity of DGs
$IC_{ESS}^{p,y,i}$	The new installed capacity of ESS
$Cap_{DG}^{p,q,y,i}$	Effective capacity of DG considering degradation impacts
$Cap_{ESS}^{p,y,i}$	Effective capacity of ESS considering leakage loss
$N_{DG}^{p,q,y,i}$	The number of DG
$\Pi_{DG}^{p,q,y,i}$	Binary variable shows if DG is installed
$\Pi_{ESS}^{p,y,i}$	Binary variable shows if ESS is installed
$DoD_{ESS}^{p,y,d,t,i}$	Depth of discharge of ESS units
$E_{ESS}^{p,y,d,t,i}$	Energy stored in battery units
$P_{DE}/P_{WT}/P_{PV}$	Diesel generator/WT/PV power output
Q_{WT}/Q_{PV}	WT/PV reactive power output
P_{PUR}/P_{SELL}	Purchasing/selling power between distributed system and grid
P_{ESC}/P_{ESD}	Charge/discharge power of ESS
μ_{de}	Binary variable for DE on/off status
$P_{flw}^{p,y,d,t,0,br+1}$	Parallel active power flow of branch b
$Q_{flw}^{p,y,d,t,0,br+1}$	Parallel reactive power flow of branch b
$V_{a,b,c}^{p,y,d,t,i}$	Bus voltage squares for phase a/b/c
$\bar{Z}_{i\to j}$	Line impedance from bus i to j
$\boldsymbol{z}_{ij}$	Line impedance matrix, denoted by the complex form of line resistance $\boldsymbol{r}_{ij}$ and reactance $\boldsymbol{x}_{ij}$
$P_{flw,a/b/c}^{y,d,t,1}$	Root branch power for phase a/b/c
$P_{unb}^{y,d,t}$	Root branch active power unbalance
P_{unb}^{max}	Hourly maximum power unbalance
$P_{unb,total}^{max}$	Total maximum power unbalance limit

I. Introduction

THE techno-economic benefits of distributed energy resources (DERs) have promoted their rapid deployment in active distribution networks (ADNs) [1]. However, the improper location and sizing of DERs would limit their benefits and even incur operational challenges for DNs. Therefore, an effective and realistic planning method to decide the size, site, type, and installation timeline of DERs is necessary.

Real-world ADNs are generally unbalanced. For example, the unbalanced line configuration in ADNs usually comprises two or single-phase laterals downstream of feeder backbones [2]. Single or two-phase loads are prevalent in ADNs, and excessive integration of renewable energy resources (RESs) into ADNs also exacerbates the three-phase unbalance [3]. However, assuming ADN as a balanced network is predominant in current DER planning literature where the DERs are installed and allocated equally in each phase [4]. This assumption will lead to unrealistic DERs planning results and may mislead the operation of the ADNS at a later stage after DER installations.

To characterize the unbalanced feature of ADNs, the three-phase power flow should be modeled. Ref. [5] calculates three-phase power flow via an iterative load flow method, however, a large number of iterations leads to a heavy computational burden. The study in [6] presents a nonlinear branch flow model to accurately solve the power flow in unbalanced ADNs, but its relaxation and convexification of the nonlinear model would intensify the computational complexity and limit its applications. Based on this branch flow model, ref. [7] proposes an approximate linearized three-phase power flow model with fast computing speed and high accuracy. It has been applied in DER planning in the literature, e.g., the optimal placement of wind power DG in unbalanced ADNs is presented in [8] with this linearized three-phase branch flow model. In [9] a robust optimization method is proposed incorporating the linearized three-phase branch flow model to assess DG capacity. A robust planning model in [10] integrates solar DG in unbalanced ADNs, considering technical, economic, and environmental perspectives. For the long-term planning problem with massive decision variables, the linearized three-phase branch flow model is preferable for alleviating the computational burden.

Apart from the more realistic modeling of the three-phase unbalanced ADNs, DER units should also be characterized accurately. DER units mainly consist of distributed generators (DGs) and energy storage systems (ESSs) Their asset health will degrade along with the service period. For instance, the fouling of the wind turbine (WT) blade leads to irreversible degradation of aerodynamic performance and conversion efficiency [11]. The power output of solar photovoltaics (PVs) will decline over time due to the corrosion and encapsulation discoloration impacts [12]. However, most of the existing planning literature neglects the DER asset health degradation.

The asset health degradation of DG units will be reflected in both efficiency and nameplate capacity decrease, which will lead to unrecoverable performance losses over time and extra costs of operation and maintenance [13]. To model such an aging process, ref. [14] presents a linear degradation model for generators' aging state, inspected by a homogeneous Poisson process. In [12], an accelerated linear degradation model is developed to assess the reliability of PVs with a single health degradation mode. The health prognostic study in [15] examines the annual capacity decline rate for WTs, which ranges from 0.118% to 0.32%. However, existing DG asset health degradation models only characterize the single DG type with specific aging modes, which cannot reflect the aging variability of multiple types of DGs over a long-term horizon. As an alternative, the Wiener degradation process with the unit-to-unit variability can catch the diverse aging rates and model the DG health degradation among various scenarios in long-term planning [13]. For ESSs, their degradation can be reflected by capacity loss after charging and discharging cycles. The study in [16] presents the whole-life-cycle planning of ESSs for providing both frequency regulation and load shifting services with the consideration of ESSs degradation. Ref. [17] demonstrates a multi-year planning method for microgrids, considering ESS power efficiency and capacity degradation. Both [16] and [17] verify that ESS aging also has a significant impact on long-term planning work in ADNs.

In addition, uncertainties from RESs and load demands should also be well addressed in DER planning. Stochastic programming (SP) is an effective approach in this regard. Ref. [18] formulates a multi-stage SP planning model to tackle the sequential DG uncertainties which are solved by a nested decomposition method. In [19], a two-stage SP approach is presented for DG planning where the random scenarios are generated by the Latin hypercube sampling method. However, both [18] and [19] handle the uncertainties separately with their independent distributions. In general, DERs are located in the nearby region of DNs, where demand variations have general features and are correlated strenuously with RES generation [20]. In this regard, the copula theory can be applied to catch this correlation. In [20], the Gumbel copula family is applied to deliberate the interdependence of WTs output and demand. Ref. [21] adopts multivariate D-vine copula to alter the copula family for uncertainties tackling in reactive power source planning. Both [20] and [21] have demonstrated the necessity of modeling the correlations among diverse uncertainties to obtain decisions more practically and accurately.

Finally, existing approaches primarily focus on the planning for DGs [22], [8], [10], [18], and [19] or ESSs [3], [16], and [23] on a separate basis, without considering their collective and mutual impacts on the ADNs. However, the individual planning approach may lead to sub-optimal decisions due to ignoring their coordination.

Given the above research gap, this paper proposes a new method for joint planning of DGs and ESSs in three-phase unbalanced ADNs considering asset health degradation and diverse correlated uncertainties. The main technical contributions are as follows:

1) A joint DER planning method is proposed to characterize the cost-benefits of DGs and ESSs concurrently while considering the three-phase unbalance in an ADN. The proposed three-phase branch flow model enables DERs to be placed among different phases and provides a more precise cost estimation.
2) The health degradation of DER units is modeled to avoid the overestimation of system adequacy over the long term. The aging cost models for DG and ESS improve the accuracy of planning results.
3) Correlated uncertainties arising from the generation of WTs, PVs, and power loads within each phase are modeled. Market volatility is also considered to account for electricity price uncertainty. Additionally, Morris Screening is utilized to select candidate DERs installation buses and reduce the problem dimension.

II. Modeling for Unbalanced Distribution Network and DER Units

A. Utility-owned DERs under consideration

This paper focuses on the utility-owned DERs, thus the proposed planning method is specifically designed for utilities to make planning decisions in the type, size, site, and installation time of DER units, with the objective of maximizing the net present value of the whole project considering investment costs and operation costs. Practical users of this method include distribution grid or microgrid owner [24], DER asset investors, etc.

Prevailing DER units are considered in this paper, including WTs, PVs, diesel generators (DEs), and battery ESSs. The DEs are characterized by rapid response times and high ramping rates. The WTs and PVs are stochastic generation resources, and the power load is with uncertain variations. Moreover, this paper takes into consideration electricity price uncertainty associated with market volatility.

B. Linear Three-phase Power Flow Model

This paper adopts a linearized three-phase branch flow model [7] for DER allocation in different phases.

Kirchhoff's voltage law is utilized for each line connected to an ordered buses pair $(i, j) \in \Xi$ and the voltage relationship can be derived as:

$$\boldsymbol{U_j} = \boldsymbol{U_i} - \boldsymbol{Z_{ij}} \boldsymbol{I_{ij}} \tag{1}$$

In (1), $\boldsymbol{U_{i/j}} = \left[U_{i/j}^a, U_{i/j}^b, U_{i/j}^c\right]^T \in \mathcal{M}^{3\times1}$ denotes the vector of three-phase voltage at bus i or bus j; $\boldsymbol{I_{ij}} = \left[I_{ij}^a, I_{ij}^b, I_{ij}^c\right]^T \in \mathcal{M}^{3\times1}$ denotes the vector of three-phase line current; $\boldsymbol{Z_{ij}} \in \mathcal{M}^{3\times3}$ denotes the line impedance matrix, derived from the complex form of line resistance $\boldsymbol{R_{ij}}$ and reactance $\boldsymbol{X_{ij}}$.The formulation of line current $\boldsymbol{I_{ij}}$ is shown in (2).

$$\boldsymbol{I_{ij}} = \boldsymbol{S_{ij}^*} \oslash \boldsymbol{V_i^*} \tag{2}$$

Substituting (2) into (1) and multiplying their complex conjugate on each side, we can then get (3), in which the apparent branch power of buses pair $(i, j) \in \Xi$ is denotes as $\boldsymbol{S_{ij}} = \left[P_{ij}^a + jQ_{ij}^a, P_{ij}^b + jQ_{ij}^b, P_{ij}^c + jQ_{ij}^c\right]^T \in \mathcal{M}^{3\times1}$. Operators $\oslash$ and $\odot$ in this approach represent the elementwise division and multiplication respectively.

$$\boldsymbol{V_j} \odot \boldsymbol{V_j^*} = \boldsymbol{V_i} \odot \boldsymbol{V_i^*} - \boldsymbol{z_{ij}}\left(\boldsymbol{S_{ij}^*} \oslash \boldsymbol{V_i^*}\right) \odot \boldsymbol{V_i^*} - \boldsymbol{z_{ij}^*}\left(\boldsymbol{S_{ij}} \oslash \boldsymbol{V_i}\right) \odot \boldsymbol{V_i} + \boldsymbol{c_{ij}}(\boldsymbol{S_{ij}}, \boldsymbol{V_i}, \boldsymbol{z_{ij}}) \tag{3}$$

The last term $\boldsymbol{\varpi_{ij}}(\boldsymbol{S_{ij}}, \boldsymbol{U_i}, \boldsymbol{Z_{ij}})$ in (3) indicates the high-order term. Then, two assumptions made in [7] are utilized for linear approximation of the three-phase branch flow:

i. The line power loss is so small that can be ignored in the model i.e., $\boldsymbol{\varpi_{ij}}(\boldsymbol{S_{ij}}, \boldsymbol{U_i}, \boldsymbol{Z_{ij}}) \ll \boldsymbol{S_{ij}}$.
ii. Voltages are nearly balanced, so we can get (4).

$$\frac{U_i^a}{U_i^b} \approx \frac{U_i^b}{U_i^c} \approx \frac{U_i^c}{U_i^a} \approx e^{j\frac{2\pi}{3}} \tag{4}$$

The assumption of nearly balanced voltages (4) is valid since the initial symmetry design of the ADNs would ensure a relatively low voltage unbalance under normal operating conditions. Moreover, periodically implemented volt/var control actions through capacity banks and on-load tap changers will also maintain the voltage magnitude close to the nominal values. Thus, the unbalanced voltage magnitude can be ignored without affecting the power flow solution accuracy.

In this regard, substituting (4) into (3) and omitting the high-order term $\boldsymbol{\varpi_{ij}}$, (3) is then simplified as (5).

$$\boldsymbol{V_j} = \boldsymbol{V_i} - \overline{\boldsymbol{Z_{ij}}}\boldsymbol{S_{ij}^*} - \overline{\boldsymbol{Z_{ij}^*}}\boldsymbol{S_{ij}} \tag{5}$$

where the voltage vector of three-phase is denoted as $\boldsymbol{V_{i/j}} = \left[\left|V_{i/j}^a\right|^2, \left|V_{i/j}^b\right|^2, \left|V_{i/j}^c\right|^2\right]^T$; the impedance matrix is $\overline{\boldsymbol{Z_{ij}}} = \Psi \odot \boldsymbol{Z_{ij}} \in \mathcal{M}^{3\times3}$; Ψ is expressed in (6):

$$\Psi=\begin{bmatrix}1 & e^{-j2\pi/3} & e^{j2\pi/3}\\ e^{j2\pi/3} & 1 & e^{-j2\pi/3}\\ e^{-j2\pi/3} & e^{j2\pi/3} & 1\end{bmatrix} \tag{6}$$

Incorporating the power balance constraints for the proposed DER planning model, the linearized three-phase branch flow can be formulated in (7)-(9). Equation (7) and (8) indicate the active and reactive power flow in ADN. Equation (9) expresses the square of the three-phase bus voltage magnitude.

$$\begin{aligned}P_{flw}^{p,y,d,t,br+1}&=P_{flw}^{p,y,d,t,br}-P_{flw}^{p,y,d,t,0,br+1}-P_{LD}^{p,y,d,t,i}+P_{DE}^{p,y,d,t,i}\\&+P_{PV}^{p,y,d,t,i}+P_{WT}^{p,y,d,t,i}+P_{BSD}^{p,q,y,d,t,i}-P_{BSC}^{p,q,y,d,t,i}\end{aligned} \tag{7}$$

$$Q_{flw}^{p,y,d,t,br+1}=Q_{flw}^{p,y,d,t,br}-Q_{flw}^{p,y,d,t,0,br+1}-Q_{LD}^{p,y,d,t,i}+Q_{WT,PV}^{p,y,d,t,i} \tag{8}$$

$$\begin{aligned}\begin{bmatrix}V_a^{y,d,t,i+1}\\V_b^{y,d,t,i+1}\\V_c^{y,d,t,i+1}\end{bmatrix}&=\begin{bmatrix}V_a^{y,d,t,br}\\V_b^{y,d,t,br}\\V_c^{y,d,t,br}\end{bmatrix}-\bar{Z}_{i\to j}\begin{bmatrix}P_{flw,a}^{y,d,t,br}-jQ_{flw,a}^{y,d,t,br}\\P_{flw,b}^{y,d,t,br}-jQ_{flw,b}^{y,d,t,br}\\P_{flw,c}^{y,d,t,br}-jQ_{flw,c}^{y,d,t,br}\end{bmatrix}\\&-\bar{Z}_{i\to j}^{*}\begin{bmatrix}P_{flw,a}^{y,d,t,br}+jQ_{flw,a}^{y,d,t,br}\\P_{flw,b}^{y,d,t,br}+jQ_{flw,b}^{y,d,t,br}\\P_{flw,c}^{y,d,t,br}+jQ_{flw,c}^{y,d,t,br}\end{bmatrix}\end{aligned} \tag{9}$$

C. Modeling for Distributed Generator Health Degradation

DG health degradation is mainly reflected in the rise in operation and maintenance (O&M) costs and the decline in nameplate capacity. Figure 1. illustrates the wind farm output showing the differences between actual and estimated generation without considering health degradation. Specifically, over the operational years, a noticeable decline in the actual capacity of WT is evident, particularly after year 5, and a total energy loss of 3782 MWh over 9 years is observed.

In this study, the aging process of DG is modeled by the Wiener degradation model [13]. The standard form of this model can be expressed in (10), where *X(t)* is the DG's degradation level at a time *t*; λ is the drift parameter, denoted the aging rate; σ_B is the standard deviation for degradation volatility; *B(t)* is the standard Brownian motion. When $\alpha=1$, the model becomes linear.

$$X(t)=X(0)+\lambda t^{\alpha}+\sigma_B B(t) \tag{10}$$

Different types of DG have varying lifetimes based on the materials, manufacture, working conditions, and physical locations. The drift parameter λ is randomized to characterize the variability in asset health degradation. The stochastic distribution of the parameter λ is shown in (11), where the expected value μ_λ and variance σ_λ of the normal distribution $N(\cdot)$ in (11) quantify the randomness of the DG aging rate. The parameter of λ and σ_B differ across various types of DG units to model distinct aging paths.

$$\lambda\sim N(\mu_\lambda,\sigma_\lambda{}^2) \tag{11}$$

To build the dynamic relationship between time t and Δt, the standard Wiener degradation model can be modified as (12). The discretization step Δt should be much smaller than DG's age. Another randomness parameter in (12), Y should be satisfied the standard normal distribution $Y\sim N(0,1)$.

$$X(t+\Delta t)=X(t)+\lambda\alpha(t)^{\alpha+1}\Delta t+\sigma_B Y\sqrt{\Delta t} \tag{12}$$

With increased DG aging, the system needs higher operational costs and more frequent maintenance. Additionally, continuous health degradation also results in a reduction of nameplate capacity, impacting the available capacity of DG generation. Hence, the equation (12) can be used to model the stochastic increase of O&M cost and decrease of the DG capacity. Specifically, with the help of the Wiener degradation model, the DG capacity drop can be expressed by (13); the unit O&M cost increment can be denoted by (14).

$$\Gamma_{cap}^{q,y}=\Gamma_{cap}^{q,y-\Delta y}+\lambda_{cap}^{q}a(y-\Delta y)^{a-1}\Delta y+\sigma_{cap}^{q}Y\sqrt{\Delta y} \tag{13}$$

$$\chi_{om}^{q,y,d,t}=\chi_{om}^{q,y,d,t-\Delta t}+\lambda_{om}^{q}b(t-\Delta t)^{b-1}\Delta t+\sigma_{om}^{q}Y\sqrt{\Delta t} \tag{14}$$

In (13), the capacity degradation level $\Gamma_{cap}^{q,y}$ of each planning phase can be defined by dynamic relationship between adjacent years, since DG health degradation is a long-term process, which is more sensitive to a yearly time scale. Combining with (13), the available operating capacity of certain DG units should drop to $(1-\Gamma_{cap}^{q,y})$*100% levels of new installed DG capacity. The maintenance cost parameter $\chi_{om}^{q,y,d,t}$ denoted in (14) represents the O&M cost increment for each DG.

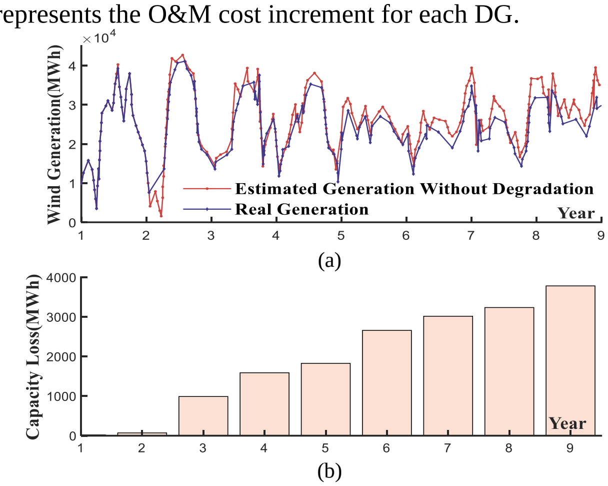

Figure 1. *(a) The health degradation comparison of the Elkhorn Valley Wind Farm between actual generation and estimated output without degradation.* [13] *(b) Annual capacity loss due to degradation*

D. Modeling for ESS Health Degradation

The health degradation of ESSs through each charging and discharging cycle can be quantified by its remaining useful life, which can be indicated by the effective cumulative ampere-hours throughput at the nominal discharging rate and the depth of discharge (DoD) before the capacity of ESS drops under 80% of its nominal capacity. The critical factor DoD denotes the percentage of ESS discharging relative to the total capacity as shown in (15). The rated ESS life is expressed in (16).

$$DoD_{ESS}^{p,y,d,t,i}=1-(E_{ESS}^{p,y,d,t,i}/E_{ESS}^{p,i,R}) \tag{15}$$

$$\varsigma_R^{p,y,i}=L_{ESS}^{p,i,R}(DoD_R^{p,i})E_{ESS}^{p,i,R} \tag{16}$$

To identify the relationship between ESS cycle life and DoD the curve fitting method can be adopted with the information provided by different manufacturers. The approximate curve demonstrating the relationship between DoD and the life cycle for Li-ion batteries is provided in Fig.2.

The mathematical formulation of the ESS life cycle is expressed in (17) where β_0 and β_1 are the life cycle curve fitting parameters [16]. Based on the descriptions above, the

ESS health degradation cost through each charging/discharging event can be expressed as (18).

$$L_{ESS}(DoD) = L_{ESS}^{p,i,R}\left(\frac{DoD_R^{p,i}}{DoD_{ESS}^{p,y,d,t,i}}\right)^{\beta_0} \cdot e^{\beta_1}\left(1-\frac{DoD_{ESS}^{p,y,d,t,i}}{DoD_R^{p,i}}\right) \tag{17}$$

$$C_{ESS_{age}}^{p,y,d,t,i} = \frac{\xi_{ESS}^{inv} L_{ESS}^{p,i,R}}{L_{ESS}^{p,y,d,t,i} DoD_R^{p,i} E_{ESS}^{p,i,R}} \tag{18}$$

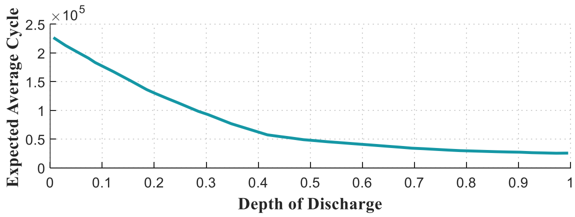

Figure 2. *The typical curve for life cycle and DoD of Li-ion batteries*

E. *Modeling for market price volatility*

Incorporating market volatility in electricity price uncertainty modeling is crucial for DER planning due to the irreversible nature of power infrastructure investment. The decisions related to DER type, site, and size require capital commitments. Market volatility, influenced by a variety of factors such as supply-demand dynamics, policy adjustments, technological advancements, and unexpected events like COVID-19, has a substantial impact on profitability and decision-making in DER planning [25]. Therefore, considering market price volatility in planning helps to support investment decisions and ensure they can adapt to fluctuating market conditions over the lifespan.

In this study, the generalized autoregressive conditional heteroskedastic (GARCH) model is utilized to capture market price volatility [26]. The GARCH uses previous information to estimate the conditional variance (volatility) of electricity prices. The GARCH model is expressed as (19), where σ_t^2 is the conditional variance (volatility); ω is constant representing the long-term average variance; α_i and β_i are coefficients for past squared residuals ε_{t-i}^2 and past conditional residuals σ_{t-j}^2. The GARCH model is denoted as GARCH (p, q), where p and q are lag orders, indicating the number of previous squared residuals and conditional variances considered.

$$\sigma_t^2 = \omega + \sum_{i=1}^{p} \alpha_i \varepsilon_{t-i}^2 + \sum_{j=1}^{q} \beta_j \sigma_{t-j}^2 \tag{19}$$

Once the forecasted conditional variance is obtained through the fitted GARCH model, the future long-term stochastic variations in electricity prices can be derived by taking the square root of the forecasted conditional variance at each time step. These variations are then scaled based on the price level to provide an estimated standard deviation, which serves as a measure of the stochastic variations in electricity prices. Based on this estimated range of stochastic variations, the uncertain price can be sampled. As the conditional variance increases, indicating higher volatility, the price fluctuations become more significant. This results in larger and more unpredictable movements in prices, leading to both higher and lower price levels. The relationship between conditional variance and electricity price captures the dynamic nature of market conditions and the impact of volatility on price behavior.

III. MATHEMATICAL MODELING FOR DER PLANNING

A. *Multistage & Multiphase Joint Planning Framework*

This paper proposes a multistage and multiphase joint planning framework for DER units, as illustrated in Fig.3. In the investment stage, the entire planning period is decomposed into multiple planning phases. The operation stage includes day-ahead operation and hourly ahead dispatch. As a two-stage decision-making problem, the investment decisions are made in the first stage considering long-term planning horizons, while operational decisions are made in the second stage considering shorter-term operational horizons.

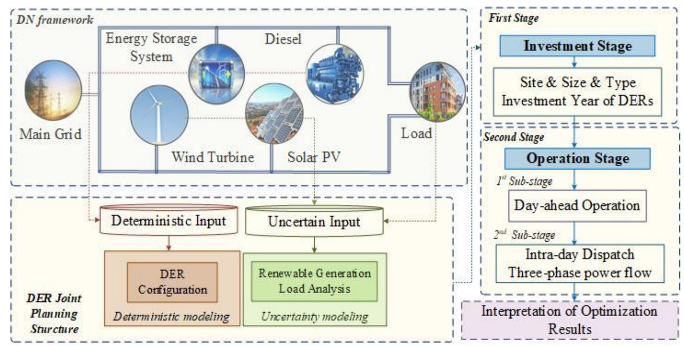

Figure 3. *The proposed DERs joint planning framework*

a) *Investment stage:* The investment decisions of both DGs and ESSs will be made in this stage, including their installed capacity and locations (including the bus and its phase to be installed), as well as planning phases. The twelve-year planning period is divided into three planning phases within the investment stage, with each planning phase spanning four years. The new DER units can only be installed in the first year of each planning phase, which is further explained in Figure 4.

b) *Operation stage:* The day-ahead decisions are made in the first operating stage, including the charging, and discharging power of the ESS and the on/off status of the DE over each dispatch interval of the next day. The intra-day decisions about DE generation output are made in the second operating stage after the uncertainties are revealed. Note that diverse and coupled uncertainties are considered in this model and the details of copula-based uncertain handling are provided in Section IV.

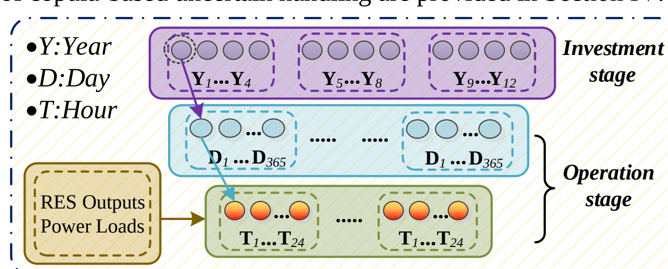

Figure 4. *Multi-phase DERs planning framework.*

B. *Mathematical Formulation*

1) Objective Function: The proposed joint planning model aims at maximizing the net present value (NPV) of the whole project over the investment and operation stages.

$$NPV = \max_{z\in\mathbb{Z}, x\in\aleph}\left[\underbrace{-F(z)}_{\text{Investment Stage}} + \underset{\text{Operation Stage}}{G(x)}\right] \tag{20}$$

$$F(z)=\sum_{y\in N_y}\frac{C_{INV}^{y}}{(1+\sigma)^{y-1}}-\frac{C_{SAL}^{N_y}}{(1+\sigma)^{N_y-1}} \tag{21}$$

$$C_{INV}^{y}=\sum_{p\in N_p}\sum_{i\in N_i}\left[\begin{array}{l}\xi_{ESS}^{inv}(IC_{ESS}^{p,y,i}-IC_{ESS}^{p,y-1,i})+\\ \sum_{q\in N_q}\xi_{DG}^{inv}(IC_{DG}^{p,q,y,i}-IC_{DG}^{p,q,y-1,i})\end{array}\right] \tag{22}$$

$$C_{SAL}^{N_y}=\sum_{y\in N_y}\gamma_{SAL}^{y}C_{INV}^{y} \tag{23}$$

Equation (20) is the objective function of the proposed model, including the capital cost at the investment stage *F(z)* in (21) and variable cost at the operation stage *G(x)* in (24) where z and x are the set of decision variables for each stage. Equation (22) denotes the investment cost for the proposed system. Equation (23) is the salvage cost of the retired DER units.

$$G(x)=\sum_{y\in N_y}\frac{C_{rev}^{y}+C_{sub}^{y}-(C_{ex}^{y}+C_{om}^{y}+C_{em}^{y}+C_{age}^{y}+C_{curt}^{y}+C_{st}^{y}+C_{sd}^{y})}{(1+\sigma)^{y}} \tag{24}$$

$$C_{rev}^{y}=\sum_{p\in N_p}\sum_{d\in N_d}\sum_{t\in N_t}\sum_{i\in N_i}\xi_{DL}^{t}P_{LD}^{p,y,d,t,i} \tag{25}$$

$$C_{sub}^{y}=\sum_{p\in N_p}\sum_{d\in N_d}\sum_{t\in N_t}\sum_{i\in N_i}\xi_{sub}^{RES}(P_{WT}^{p,y,d,t,i}+P_{PV}^{p,y,d,t,i}) \tag{26}$$

$$C_{ex}^{y}=\sum_{p\in N_p}\sum_{d\in N_d}\sum_{t\in N_t}\sum_{i\in N_i}(\xi_{pur}^{t}P_{PUR}^{p,y,d,t,i}-\xi_{sell}^{t}P_{SELL}^{p,y,d,t,i}) \tag{27}$$

$$C_{om}^{y}=\sum_{p\in N_p}\sum_{d\in N_d}\sum_{t\in N_t}\sum_{i\in N_i}\left[\begin{array}{l}\chi_{om,ESS}(p_{ESC}^{p,y,d,t,i}+p_{ESD}^{p,y,d,t,i})\\ +\sum_{q\in N_q}\chi_{om,DG}^{q,y,d,t}P_{DG}^{p,q,y,d,t,i}\end{array}\right] \tag{28}$$

$$C_{em}^{y}=\sum_{p\in N_p}\sum_{d\in N_d}\sum_{t\in N_t}\sum_{i\in N_i}(\xi_{em}^{DE}P_{DE}^{p,y,d,t,i}-\xi_{em}^{pur}P_{PUR}^{p,y,d,t,i}) \tag{29}$$

$$C_{age}^{y}=\sum_{p\in N_p}\sum_{d\in N_d}\sum_{t\in N_t}\sum_{i\in N_i}C_{ESS_{age}}^{p,i,y,d,t}\left(P_{ESC}^{p,y,d,t,i}+P_{ESD}^{p,y,d,t,i}\right) \tag{30}$$

$$C_{curt}^{y}=\sum_{p\in N_p}\sum_{d\in N_d}\sum_{t\in N_t}\sum_{i\in N_i}\left[\begin{array}{l}\xi_{cur}^{WT}\left(P_{WT,real}^{p,y,d,t,i}-P_{WT}^{p,y,d,t,i}\right)+\\ \xi_{cur}^{PV}\left(P_{PV,real}^{p,y,d,t,i}-P_{PV}^{p,y,d,t,i}\right)\end{array}\right] \tag{31}$$

$$C_{st}^{y}=\sum_{p\in N_p}\sum_{d\in N_d}\sum_{t\in N_t}\sum_{i\in N_i}\max\left\{0,\mu_{de}^{p,y,d,t,i}-\mu_{de}^{p,y,d,t-1,i}\right\}C_{DE}^{up} \tag{32}$$

$$C_{sd}^{y}=\sum_{p\in N_p}\sum_{d\in N_d}\sum_{t\in N_t}\sum_{i\in N_i}\max\left\{0,\mu_{de}^{p,y,d,t-1,i}-\mu_{de}^{p,y,d,t,i}\right\}C_{DE}^{down} \tag{33}$$

Equation (25) denotes the revenue from selling power to local customers within the ADN; (26) shows the subsidy for WTs and PVs utilization; (27) is the power transaction cost between the DN and the main grid; Equation (28) represents the maintenance cost which will change along with DG health degradation, modeled in (14); (29) is the gas emission cost; (30) shows the battery storage degradation cost combined with (18) ; Equation (31)-(33) denote the RES power curtailment cost, DE start-up, and shut-down cost respectively.

2) Constraints:

The constraints for the planning stage are as follows.

$$IC_{DG}^{p,q,y,i}=N_{DG}^{p,q,y,i}IC_{DG}^{q,unit}+IC_{DG}^{p,q,y-1,i} \tag{34}$$

$$\Pi_{DG}^{p,q,y,i}IC_{DG}^{q,MIN}\le IC_{DG}^{p,q,y,i}\le\Pi_{DG}^{p,q,y,i}IC_{DG}^{q,MAX} \tag{35}$$

$$\sum_{i\in N_i}IC_{DG}^{p,q,y,i}\le IC_{DG,ALL}^{p,q} \tag{36}$$

$$\Pi_{ESS}^{p,y,i}IC_{ESS}^{MIN}\le IC_{ESS}^{p,y,i}\le\Pi_{ESS}^{p,y,i}IC_{ESS}^{MAX} \tag{37}$$

$$\sum_{i\in N_i}IC_{ESS}^{p,y,i}\le IC_{ESS,ALL}^{p} \tag{38}$$

Equation (34) denotes the newly installed capacity of different types of DGs, such as DEs and WTs should have discrete unit size; (35) and (36) means the hosting limits of new DGs installed capacity for each bus and for the system; Equation (37) and (38) means the size limits of new installed ESS for each bus and for the system, respectively.

$$\sum_{i\notin N_i}\Pi_{DG}^{p,q,y,i}+\Pi_{ESS}^{p,y,i}=0 \tag{39}$$

$$if\ \ y\in N_y^{INV}\begin{cases}IC_{DG}^{p,q,y,i}\ge IC_{DG}^{p,q,y-1,i}\\ IC_{ESS}^{p,y,i}\ge IC_{ESS}^{p,y-1,i}\end{cases} \tag{40}$$

$$if\ \ y\notin N_y^{INV}\begin{cases}IC_{DG}^{p,q,y,i}=IC_{DG}^{p,q,y-1,i}\\ IC_{ESS}^{p,y,i}=IC_{ESS}^{p,y-1,i}\end{cases} \tag{41}$$

Equation (39) indicates the DGs and ESSs can only be installed at the selected candidate buses; (40) shows the installation of DERs can only happen in the first year of each planning phase, and (41) means for the remaining years of each planning phase, the DERs capacity should remain the same.

$$\begin{aligned}Cap_{DG}^{p,q,y,i}=&\sum_{m=1}IC_{DG}^{p,q,y,i}\left(1-\Gamma_{cap}^{q,y}\right)+\\ &\sum_{m\in N_y^{INV}}\left(IC_{DG}^{p,q,m,i}-IC_{DG}^{p,q,m-1,i}\right)\left(1-\Gamma_{cap}^{q,y-m}\right)\end{aligned} \tag{42}$$

$$Cap_{ESS}^{p,y,i}=\sum_{m\in N_y^{INV}}\left(IC_{ESS}^{p,m,i}-IC_{ESS}^{p,m-1,i}\right)\left(1-\beta_{LL}\right)^{y-m} \tag{43}$$

Equation (42) denotes the capacity drop of DG units caused by the asset aging effect, as determined in (13). The available capacity of DGs installed in the first planning phase is determined by multiplying the installed capacity by the aging rate. In subsequent planning phases, the available DG capacity is calculated by multiplying the newly installed DG capacity within each planning phase with the aging rate corresponding to the number of years since installation; (43) is the available capacity of ESSs considering the calendar loss of capacity [23].

$$\beta_{de}^{\min}\mu_{de}^{p,y,d,t,i}Cap_{DG}^{p,q,y,i}\le P_{DE}^{p,y,d,t,i}\le\beta_{de}^{\max}\mu_{de}^{p,y,d,t,i}Cap_{DG}^{p,q,y,i} \tag{44}$$

$$R_{DE}^{down}\Delta t\le P_{DE}^{p,y,d,t,i}-P_{DE}^{p,y,d,t-1,i}\le R_{DE}^{up}\Delta t \tag{45}$$

$$\left[P_{WT}^{p,y,d,t,i},P_{PV}^{p,y,d,t,i}\right]\le\left[P_{WT,REAL}^{p,y,d,t,i},P_{PV,REAL}^{p,y,d,t,i}\right] \tag{46}$$

$$\left[P_{ESC}^{p,y,d,t,i},P_{ESD}^{p,y,d,t,i}\right]\begin{cases}\ge\left[\beta_{esc}^{\min},\beta_{esd}^{\min}\right]Cap_{ESS}^{p,y,i}\\ \le\left[\beta_{esc}^{\max},\beta_{esd}^{\max}\right]Cap_{ESS}^{p,y,i}\end{cases} \tag{47}$$

$$P_{ESC}^{p,y,d,t,i}\cdot P_{ESD}^{p,y,d,t,i}=0 \tag{48}$$

$$\gamma_{ess}^{\min}Cap_{ESS}^{p,y,i}\le E_{ESS}^{p,y,d,t,i}\le\gamma_{ess}^{\max}Cap_{ESS}^{p,y,i} \tag{49}$$

$$E_{ESS}^{p,y,d,t,i}=(1-\tau_{es})E_{ESS}^{p,y,d,t-1,i}+(P_{ESC}^{p,y,d,t,i}\eta_{esc}-P_{ESD}^{p,y,d,t,i}/\eta_{esd})\Delta t \tag{50}$$

$$E_{ESS}^{p,y,d,0,i}=E_{ESS}^{p,y,d,N_t\Delta t,i} \tag{51}$$

Equation (44) and (45) are the power boundary and the ramping rate limits for DEs to ensure their power output and power variations remain within the allowable range; (46) denotes the RESs generation cannot exceed the available resources; (47)-(51) are the operational constraints for ESS; (47) denotes the charging/discharging power should be within the capacity limits; (48) ensures that charging/discharging events do not occur simultaneously; (49) is the ESS energy stored limits and (50) relates to the relationship between stored energy and charging or discharging power; (51) enforces the scheduling flexibility for ESSs across dispatch periods, where the starting and ending energy levels are equal.

$$\begin{bmatrix} \left| P_{flw,a}^{y,d,t,1} - P_{flw,b}^{y,d,t,1} \right| \\ \left| P_{flw,b}^{y,d,t,1} - P_{flw,c}^{y,d,t,1} \right| \\ \left| P_{flw,c}^{y,d,t,1} - P_{flw,a}^{y,d,t,1} \right| \end{bmatrix} \le P_{unb}^{y,d,t} \le P_{unb}^{\max} \quad (52)$$

$$\sum_{d\in N_d} \sum_{t\in N_t} P_{unb}^{y,d,t} \le P_{unb,total}^{\max} \quad (53)$$

$$\left(P_{flw}^{p,y,d,t,1}\right)^2 + \left(Q_{flw}^{p,y,d,t,1}\right)^2 \le \left(S_{TF}^{\max}\right)^2 \quad (54)$$

$$V_{\min}^2 \le \left[V_a^{y,d,t,i}, V_b^{y,d,t,i}, V_c^{y,d,t,i}\right] \le V_{\max}^2 \quad (55)$$

Equation (52) and (53) are the power unbalance constraints for the operation stage, indicating the root branch unbalance at each time interval and the overall power unbalance should be within the pre-defined limits, respectively; (54) denotes the root branch apparent power should be within the power limit of the transformer; (55) limits the bus voltage of each phase within the safety range [3]. The linearized power flow model for an unbalanced system is given in (7)-(9) [7].

IV. Solution Methods

A. Candidate Bus Selection

For the DERs planning in unbalanced ADNs, the model scale can be very large. To reduce the model dimension and construct a moderate optimization model, the candidate buses should be identified for DERs. In this paper, the Morris Screening is utilized to identify the candidate bus by evaluating the most influential parameters through the construction of a multi-dimensional semi-global trajectory for search space [28]. The rationale is that a single variable will be changed by a magnitude of $\Delta\varpi$ at each time step. An elementary impact on the change of $\Delta\varpi$ is in (56).

$$\Psi^{\varpi,i} = \frac{f(x^{\varpi,i} + \Delta\varpi) - f(x^{\varpi,i})}{\Delta\varpi}, \forall i \in \Xi, \varpi \in N_{\varpi} \quad (56)$$

The term $f(x^{\varpi,i})$ represents the objective function from the operation module of the proposed system in (24), which is subject to the operational constraints in (7)-(9) and (44)-(55). Equation (56) quantifies the evaluation outcome for candidate bus $i \in \Xi$, when the DG capacity of $x^{\varpi,i}$ has been installed. After each simulation, the variable $x^{\varpi,i}$ will be changed by $\Delta\varpi$.

The criterion to help identify candidate bus is the mean value μ_{cs}^i and standard deviation σ_{cs}^i of this elementary impact, expressed as (57) and (58).

$$\mu_{cs}^i = \left(\sum_{\varpi=1}^{N_{\varpi}} \left|\Psi^{\varpi,i}\right|\right) \Big/ N_{cs} \quad (57)$$

$$\sigma_{cs}^i = \sqrt{\left(\sum_{\varpi=1}^{N_{\varpi}} \left(\left|\Psi^{\varpi,i}\right| - \mu_{cs}^i\right)^2\right) \Big/ N_{cs}} \quad (58)$$

In (57), the mean value is the sensitivity strength between the different buses and evaluation results. The smaller the μ_{cs}^i value is, the less impact of DGs on ADNs will have. Equation (58) measures non-linear or interaction effects of the i^{th} input. A small σ_{cs}^i indicates low variations in the impact of elementary perturbation across the input range, implying a linear relationship between input and output. In the planning, the original model is inherently complex. The selection of candidate buses for network planning aims to simplify the problem and streamline the decision-making process [21]. However, considering the non-linear impacts can introduce unnecessary challenges and undermine the assumptions of linearity. Hence, the ideal conditions of candidate buses are expected to have a high and linear impact.

B. Copula-based stochastic uncertainty modeling

a) Copula Formulation

To capture the strenuous correlations among diverse uncertainties (load demand, WT, and PV power outputs), the copula function is utilized in this paper. Copula denotes a multivariate cumulative distribution of each variable with uniform marginals in the unit interval [0, 1] [21]. Concerning an N-dimensional random input vector $A = \{A_1, A_2, \dots, A_N\}$ with marginals$\{F_{A_1}, F_{A_2}, \dots, F_{A_N}\}$ is associated with a copula C to indicate their joint cumulative distribution function F_A in (59).

$$F_A(a) = C(F_{A_1}(a_1), F_{A_2}(a_2), \dots, F_{A_N}(a_N)) \quad (59)$$

Thus, differentiating (59), the joint probability distribution function of vector $A = \{A_1, A_2, \dots, A_N\}$ can be derived from (60) where the copula density function is indicated as (61). The conditional density functions can be formulated as (62)

$$f_A(x) = c(F_{A_1}(a_1), F_{A_2}(a_2), \dots, F_{A_N}(a_N)) \prod_{j=1}^{N} f_{A_j}(a_j) \quad (60)$$

$$c(a) = c(\kappa_1, \kappa_2, \dots, \kappa_N) = \frac{\delta^N C(\kappa_1, \kappa_2, \dots, \kappa_N)}{\delta\kappa_1, \kappa_2, \dots, \kappa_N} \quad (61)$$

$$\begin{aligned} f_{1|2,\dots,N}\left(a_1 \middle| a_1, \dots, a_N\right) &= f_A(a) \Big/ \prod_{j=1}^{N} f_{A_j}(a_j) \\ &= c(F_{A_1}(a_1), F_{A_2}(a_2), \dots, F_{A_N}(a_N)) \cdot f_1(a_1) \end{aligned} \quad (62)$$

For high-dimension problems, construction and application of various pair copulas become essential. Gaussian and Gumbel copula families, represented by cumulative distribution functions (63) and (64), are used to model both linear and non-linear correlations, while accommodating tail dependencies that often arise due to the intermittent nature of renewable energy sources [29][30]. Based on copula-based scenario generation, the hidden correlations between renewable energy sources and power load can be revealed with the support of pair copulas.

$$C_{Gau} = \varphi_{2;\alpha}(\varphi^{-1}(k), \varphi^{-1}(t))^{(\mu)}, \alpha \in (-1,1) \quad (63)$$

$$C_{Gum} = \exp(-((-\log k)^{\alpha} + (-\log t)^{\alpha})^{\frac{1}{\alpha}}), \alpha \in [1, \inf) \quad (64)$$

b) Stochastic optimization model

To handle the uncertainties, the operation stage in the proposed model is further decomposed into day-ahead operation substage and intra-day dispatch substage. For the day ahead substage, decisions are made based on the input prediction and operation parameters, involving 24-hour ESSs charging or discharging power decisions, and the on/off status of DEs. The uncertainties are not revealed in the day-ahead stage. The second substage covers a shorter operation timescale (the unit dispatch interval is set as one hour), making the decisions after revealing the real-time uncertainties [19]. The fast response generators, DEs, are dispatched to maintain the real-time power balance considering the power exchange with the main grid.

In this study, we utilize the copula-based two-stage stochastic optimization approach. This approach involves generating scenarios that capture the correlations between variations in WTs and PV outputs, as well as power load of the system. Additionally, the electricity price uncertainty is incorporated, considering the market volatility. To reduce the problem scales, the simultaneous backward reduction method is utilized to select the representative scenarios. The overall stochastic optimization can be formed as (65).

$$
\begin{aligned}
obj = \underset{\alpha, y_1, y_2, \ldots, y_s}{Min} & \left[H(\alpha) + \sum_{s=1}^{N_s} p_s \cdot L(y_s) \right] \\
s.t. \quad & \alpha \in CD_\alpha \,|\, z \\
& y_s \in CL(\alpha, \beta_s), \forall s \in N_s
\end{aligned} \tag{65}
$$

In (65), $H(\boldsymbol{\alpha})$ is the objective of investment stage and the day ahead operation substage, related to (21)-(23), (27), (28) and (30) where $\boldsymbol{\alpha}$ denotes all the corresponding decisions discussed above; s is the index of the representative scenarios; CD_α is the constraint set, involving (34)-(51), related to decision $\boldsymbol{\alpha}$; N_s is number of total scenarios; p_s is probability of scenario; $L(y_s)$ is the objective of intra-day dispatch substage after revealing the uncertainties, consisting of (29) and (31), in which y_s is the decision variable for DEs dispatch. $\mathrm{E}\,[L(y_s)]$ shows the expectation cost from dispatchable DE generators. β_s denotes the uncertainties in the stochastic model; $CL(\alpha, \beta_s)$ is the constraints corresponding to the decision y_s, including (7)-(9) and (44)-(55).

V. Case Study

A. Test System

The proposed joint DERs planning model is validated via an IEEE 34-bus three-phase system, whose single-line diagram can be shown in Fig.5 [31]. Detailed information on the system data and the unbalanced load data for each phase in the test system can be referred to [32]. ESSs and PVs can be installed on buses (808, 832, 844, 848, 860, 840) with red and purple dots in Fig. 5., refer to [3]. The candidate buses for other types of DGs are selected by Morris Screening shown as green dots and purple dots in Fig.5, consisting of buses (808, 814, 818, 826, 832, 842). In this study, we have selected three typical days from the summer, winter, and transition seasons (spring and fall). The forecasting profiles of all the uncertain resources are shown in Fig.6. The dispatch period is 4 hours to reduce the computation burden. The detailed parameters of DGs and ESSs are given in Table I, including investment and maintenance costs, and the newly installed capacity limits of DERs for each candidate bus and system. The energy tariffs for the proposed system and the other cost parameters in the objective functions are provided in Table II, extracted from [19].

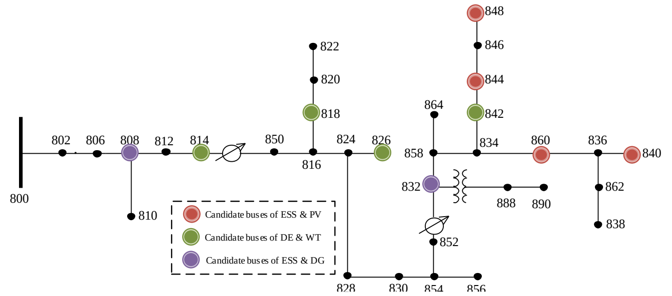

Figure 5. *IEEE 34-bus distribution system topology*

The project lifetime is 12 years with four years as a planning phase. The bus voltage limit is set as [0.95, 1.05] p.u. The maximum allowable power unbalance for each dispatch period P_{unb}^{max} is set as 0.17 p.u. The profile of load variations and renewable generations can be found in [33][34]. It is important to note that the effectiveness of the proposed method does not rely on the data inputs and parameter settings. Any real-world data can be used in this regard.

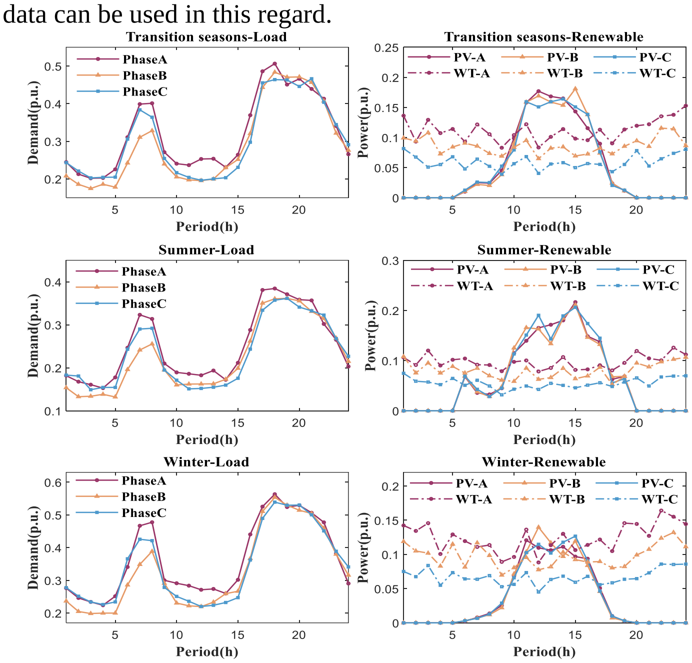

Figure 6. *Forecasted demand and RES output for three typical days*

TABLE I. Technical details of DGs and ESSs

Type	Cost/($/kW)		Capacity/(kW)	
	Invest	Maintain	Bus limits	System limits
DE	1121	0.0287	0/480	0/1900
WT	2012	0.005	0/200	0/1800
PV	1792	0.00912	0/200	0/1600
ESS	385	0.0077	0/240	0/2160

TABLE II. Energy tariffs and cost parameter

Parameter	Price ($/kW)	Parameter	Price ($/kWh)	Period (h)
ξ_{DL}^{t}	0.225	ξ_{pur}^{t}	0.0768	0-6,23-24
ξ_{sub}^{RES}	0.45		0.12765	6-8,11-17
$\xi_{cur}^{WT}/\xi_{cur}^{PV}$	0.005		0.1696	8-11,17-22
ξ_{em}^{DE}	0.026	ξ_{sell}^{t}	0.05144	0-24
ξ_{em}^{pur}	0.0889			

The candidate bus selection for DE and WT buses based on the Morris screening method is shown in Figure 7. The mean value μ_{cs}^{i} is the key determinant for candidate bus selection while the standard deviation σ_{cs}^{i} enables to support the decisions in second place. For instance, the mean value of bus 806 and bus 842 is extremely close, however, bus 806 is discarded due to its large value of σ_{cs}^{i}.

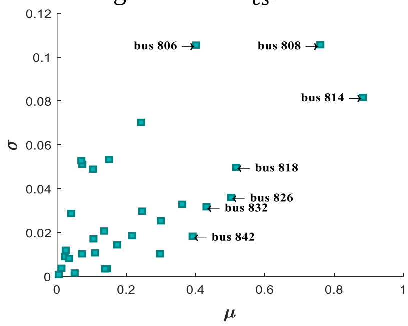

Figure 7. *Candidate bus selection results*

The DG aging parameter in the Wiener degradation model is given in Table III. The probability distribution curve for drift parameter λ_{cap} and λ_{om} with the parameter provided in Table III are shown in Fig.8. Based on (13)-(14), the capacity drop level and maintenance cost variations by asset health degradation are also presented in Fig.8, in which the capacity drop level increases sharply after 10 years and the maintenance cost for WT has a huge growth after 12 years. More detailed information can be found in [13]. The parameters for ESS aging are $L_{ESS}^{p,i,R}$= 2190, β^0= 4580, β^1=1.98 and $DoD_R^{p,i}$= 0.8 [16].

TABLE III. DG AGING PARAMETER IN WIENER DEGRADATION MODEL

Type	Aging rate	Aging volatility
DE	$\lambda_{cap}^{DE} \sim N(0.0043,0.0005)$ $\lambda_{om}^{DE} \sim N(0.000027,0.000003)$	$\sigma_{cap}^{DE} = 0.0045$ $\sigma_{om}^{DE} = 0.000002$
WT	$\lambda_{cap}^{WT} \sim N(0.0138,0.0004)$ $\lambda_{om}^{WT} \sim N(0.00085,0.000023)$	$\sigma_{cap}^{WT} = 0.01$ $\sigma_{om}^{WT} = 0.00001$
PV	$\lambda_{cap}^{PV} \sim N(0.0048,0.0005)$ $\lambda_{om}^{PV} \sim N(0.00002,0.000002)$	$\sigma_{cap}^{PV} = 0.004$ $\sigma_{om}^{PV} = 0.0000012$
All types of DG: *a=1, b=1*		

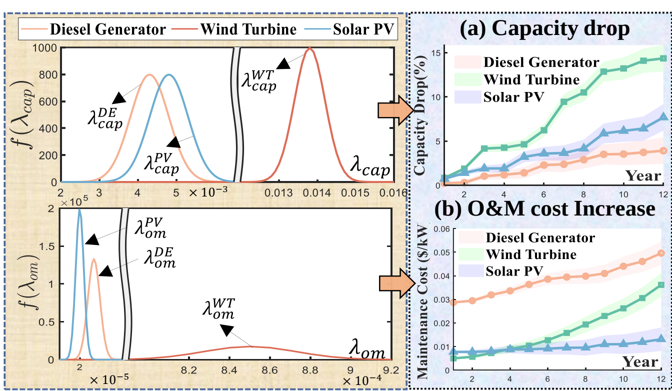

Figure 8. *The drift parameter probability distribution and the capacity drop level and maintenance cost increase by asset health degradation.*

The historical electricity price data spanning 2015 to 2020 [27] is utilized to fit the GARCH model, aiming to capture the market price volatility. Owing to data availability, the model is validated using data from 2020. The validation results for the one-month market volatility in 2020 are depicted in Fig. 9. It can be seen that the forecasted volatility closely tracks the trend of actual market volatility. The model's quantitative evaluation, indicated by a mean absolute percentage error (MAPE) of 18.15%, falls within an acceptable range. It is crucial to highlight that forecasting market volatility is not the primary focus of this study. For more precise predictions of electricity price volatility, advanced forecasting methods available in the literature can be employed.

The forecasted market price volatility for the next 12 years is provided in Fig.10, based on the fitted GARCH model (19). The conditional variance derived from (19) indicates price volatility. In Fig. 10, it can be observed that the overall trend of volatility is increasing over the years. Stochastic variations in electricity prices are estimated by taking the square root of the forecasted volatility and scaling it as a percentage relative to the predicted electricity price level [19]. This scaled volatility is the electricity price variations that account for the uncertain nature of market conditions. Thus, the obtained stochastic variations enable the sampling of uncertain electricity prices, capturing the potential fluctuations in price over the 12-year forecast period.

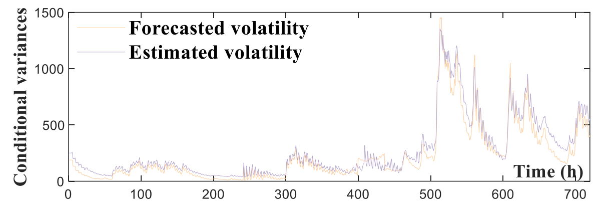

Figure 9. *Validation results for market volatility in 2020*

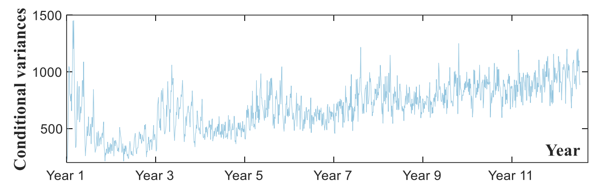

Figure 10. *Forecasted conditional variance for the next twelve years.*

The discount rate is 6% and the annual load growth rate is assumed to be 6.7% [23]. The stochastic variations of renewable generation and power demand are set at 30% and 10%. All the case studies are conducted on an Intel(R) Core (TM) i5-10500U CPU @ 3.10GHz PC with 16G RAM and solved by Gurobi through Pyomo (version 6.0.1) package on Python.

B. *Simulation results in the investment stage*

The simulation is conducted with five representative scenarios which are reduced from 1000 randomly sampled scenarios considering multiple uncertainties. The planning results for DEs and WTs are presented in Table IV. Results for ESSs and PVs are summarized in Table V.

The results indicate the total installed capacity for DER units each year. DERs can only be installed during the first year of each planning phase, while the capacity of DERs remains constant for the subsequent years of that planning phase. The following findings can be observed from the simulation results:

(i). The results present an increasing trend in DER installation from year 1 to year 12 to meet the annually growing demand. The renewable-based DER units have been installed in the earlier planning phase, especially PV installations are one-time investments to maximize the overall profits. The reason is that the operation cost of RESs is relatively low, and the RESs curtailment is supposed to be avoided, so installing RESs in the first year can maximize their benefits.

(ii). ESSs are extensively invested in ADNs during the final planning phase, while no ESS installations occur in the first planning phase. ESSs are crucial for peak shaving, but when the peak load is low, the profits obtained from energy shifting between valley and peak prices do not justify the capital cost of

ESS installation. Conversely, in the last planning phase, with a significant increase in power demand, ESSs are utilized to efficiently shift the load and maintain the power balance.

(iii). For the siting results of DERs, most ESSs are located closely with RESs. The unbalanced nature can also be captured since ESS is installed on the same ADN phase together with RESs for most cases. For example, for years 5-8, ESS is located on the same phase with PV on buses 808 and 860; ESS on bus 860 is quite close to WT on bus 842 and both are installed on phases A and C.

TABLE IV. DG DEPLOYMENT RESULTS FOR DE AND WT GENERATORS

Year	Phase /bus	DE (kW)				WT (kW)			
		808	814	826	842	808	814	826	842
1-4	A	0	50	0	0	50	200	0	170
	B	150	0	0	0	200	50	70	0
	C	80	0	280	0	0	0	0	200
5-8	A	0	240	120	0	50	200	0	200
	B	180	0	0	270	200	70	70	0
	C	80	0	0	250	40	0	0	200
9-12	A	0	240	120	160	50	200	0	200
	B	200	0	0	400	200	70	70	0
	C	90	0	330	290	40	0	0	200

TABLE V. ESS AND PV GENERATORS DEPLOYMENT RESULTS

Year	Phase/ bus	ESS (kWh)				
		808	860	840	844	848
1-4	A	0	0	0	0	0
	B	240	0	0	0	0
	C	0	240	0	0	0
5-8	A	0	0	0	0	0
	B	240	0	0	0	0
	C	0	240	0	0	0
9-12	A	0	240	0	240	240
	B	240	0	240	0	240
	C	0	240	240	240	0
Year	Phase	PV (kW)				
1-12	A	200	0	0	0	165
	B	183	0	0	200	0
	C	0	180	200	0	0

C. Simulation results in the operation stage

Copula theory is implemented to produce 1000 scenarios of the RES power generation and load demand, which are then reduced to 5 typical scenarios for each typical day. To illustrate the correlation between WT, PV, and power load, the scatter plot is provided in Fig.11, presenting 300, 500, and 1000 samples generated from the dataset during the peak periods of PV generation in Spring. Fig.11 clearly shows that samples of various sizes cluster predominantly in the center of the figure, indicating strong correlations between diverse uncertainties and showing a high degree of similarity of these scenarios. Based on this clustering behavior, 5 representative scenarios are used to capture significant variations while maintaining accuracy.

To indicate the effectiveness of the proposed approach in the operation stage, Fig. 12 presents the dispatch results in unbalanced ADNs for the typical day in the transition season of the final planning year (2034).

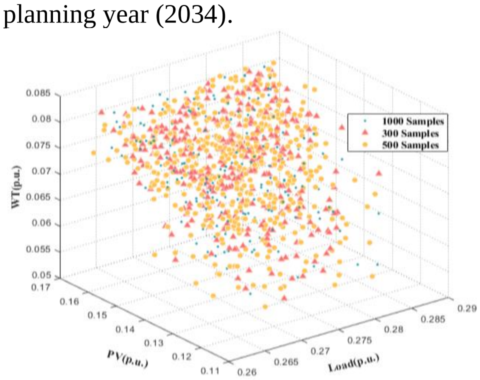

Figure 11. *Comparison of different numbers of samples via copula theory*

Fig.12 demonstrates the effective coordination of all DERs in supplying loads while minimizing the operation cost. The RESs operate at their maximum power output without curtailment due to their low operation cost. Notably, excessive selling and charging occur during the peak solar generation period (8-16h) to generate profit. The ESSs successfully achieve load peak shaving and system cost reduction by charging during the period with the lowest transaction price (2-6h) and discharging during peak-load periods (18-22h) to maintain the power balance and minimize utility purchasing costs. Additionally, the limited frequency of ESSs charging and discharging is due to considerations of degradation cost, as explained in equation (29). These results highlight the efficient and cost-effective operation of DERs, verifying the optimal decisions made in the DERs planning process.

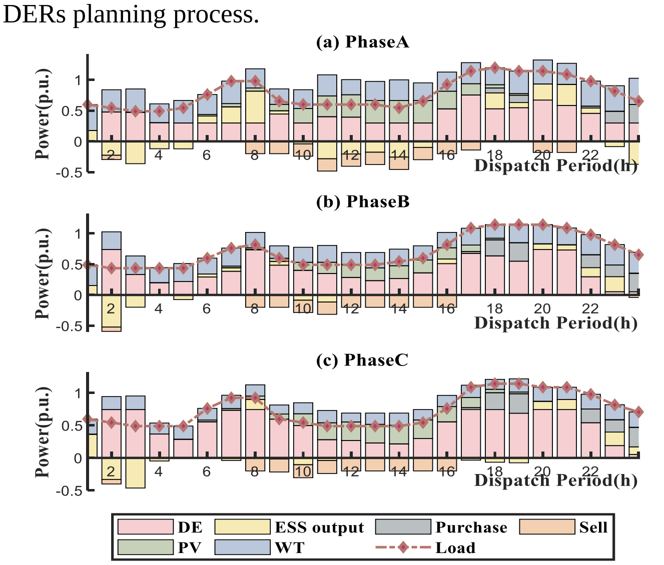

Figure 12. *Simulation results for operation stage in year 2034-Spring/Fall*

From the input prediction in Fig.6 and the installation results, the maximum installed capacity of RES is observed in Phase A, surpassing Phase B and Phase C. The operation results further confirm this trend since the charging and discharging times and power of ESSs in phase A are the highest among the three phases. This finding verifies that ESSs are more likely to operate in the phase with a significant output of RESs.

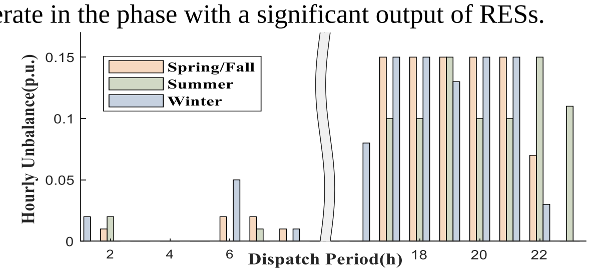

Figure 13. *Results of hourly unbalance for three typical days*

Fig.13 displays the hourly unbalance results for three typical days, using the index defined in (66) to quantify the three-phase power unbalance. It is evident that the highest unbalance occurs when the load reaches its peak during the day, primarily due to significant power exchange from the grid and ESSs discharging to meet the peak demand. It should be noted that the three-phase unbalance remains within the predefined limits for all the considered days.

$$Hourly\ unbalance = \sum_{t\in N_t} P_{unb}^{y,d,t} / N_t \quad \forall y \in N_y, d \in N_d \quad (66)$$

The solving time of the proposed DERs joint planning model and candidate bus selection process are 84528 and 2359 seconds, respectively. The operation stage needs 656 seconds.

D. Comparison for Different Methods

To fully demonstrate the effectiveness of our proposed method, three planning benchmark methods are compared for unbalanced ADNs:

M1**:** Deterministic DERs joint planning, i.e., the RES output, demand, and electricity price are accurately known [35].

M2**:** ESS planning with pre-defined DGs installation. The DG installations are input parameters rather than variables [23].

M3**:** DGs planning with pre-defined ESS installation. The capacity and location of ESSs are predetermined and installed at the beginning of the project [19].

Simulation results of all the compared methods and our proposed method are presented in TABLE VI. indicating that:

(i). For ***M1***, without consideration of intra-day readjustment, planning results have less profit and lower investment cost compared to the proposed method, due to the omission of potential revenue and the optimality of DER installations. By considering uncertainties, decision-making can be informed by probabilistic scenarios, resulting in more efficient and robust DER utilization in the face of uncertain conditions.

(ii). In **M2**, where all DGs are installed in the first year, additional expenses are incurred due to higher operating costs and lower salvage costs from early installations. Similarly, in **M3**, the cost difference apparently arises from fewer ESS installations in the early phases, resulting in higher investment costs. However, the proposed method achieves higher profits and lower investment costs, despite the longer solution time resulting from the increased complexity of DERs joint planning in the unbalanced ADNs.

(iii). The proposed method reports lower hourly unbalance compared to **M1** and **M3**, although it is slightly higher than **M2**. This difference can be attributed to the early installation of DGs, which reduces the need for power transactions with the main grid. The power exchange at the root bus has a significant influence on the three-phase unbalance. However, it is important to note that all methods comply with the pre-defined unbalance constraints.

TABLE VI. SIMULATION RESULTS OF ALL COMPARED METHODS

Item	M1	M2	M3	Proposed Method
Objective $\times 10^6/(\$)$	4.06	4.39	3.76	4.75
Investment cost $\times 10^6/(\$)$	3.01	3.86	4.29	3.73
Hourly unbalance $(p.u.)$	0.0489	0.0322	0.0436	0.0412
Solution time (hr)	1.56	8.89	11.31	23.48

E. Comparison with a balanced network

Additional simulation tests are conducted on a balanced system to compare the planning outcomes with the unbalanced system. To maintain consistency, the IEEE standards 34-bus system from [31] is modified by transitioning single or two-phase line configurations to identical three-phase lines and distributing unbalanced loads evenly across all three phases. The operation stage test is conducted in the proposed network based on the obtained DER installation decisions from the balanced network configuration.

Table VII presents the comparison results between the balanced and unbalanced network. In the investment stage, compared with the balance network assumption, the DERs planning in the unbalanced network has slightly lower investment costs, and significantly less operation cost and much lower unbalance index during the operation. It is noted that the final year DER installation decisions varied significantly between the balanced and unbalanced networks. In the unbalanced network, DGs capacity is 12.9% lower, while ESS capacity is 20.4% higher compared to results on the balanced network. These variations in DER planning results directly affect network power flow and network operation: the operation cost based on the balanced network decisions is 5.24% higher than the proposed approach, and hourly unbalance index is twice higher. This further confirms the proposed approach's ability to reduce network unbalance and enhance profitability for utilities.

TABLE VII. RESULTS COMPARISON WITH BALANCED NETWORK

Item		Balance network	Unbalance network
Investment Stage	Objective $\times 10^6/(\$)$	4.741	4.758
	Investment cost $\times 10^6/(\$)$	3.756	3.737
Operation Stage	Operation cost $/(\$)$	7430	7060
	Hourly unbalance $(p.u.)$	0.0805	0.0412

Network	DE/ (kW)	WT/ (kW)	PV/ (kW)	ESS/ (kWh)
Balance	2280	1050	1149	1720
Unbalance	1810	1030	1127	2160

F. Sensitivity Analysis for DG Health Degradation Parameter

To assess the impact of DGs' health degradation on the system, the sensitivity analysis is conducted under different DGs' health degradation degrees. The DG health degradation parameters are capacity drop degree $\Gamma_{cap}^{q,y}$ and the O&M cost-increasing degree $\chi_{om}^{q,y,d,t}$ in (13) and (14). The sensitivity index k is introduced to show the changes in $\Gamma_{cap}^{q,y}$ and $\chi_{om}^{q,y,d,t}$, whose updated value is calculated by (67) and (68). The sensitivity results, ranging from 10% to 50% for k, are shown in Fig.14. The proposed method when k=0 is also presented to highlight the variations.

$$\left(\Gamma_{cap}^{q,y}\right)_{new} = \Gamma_{cap}^{q,y} \cdot (1+k) \quad (67)$$

$$\left(\chi_{om}^{q,y,d,t}\right)_{new} = \chi_{om}^{q,y,d,t} \cdot (1+k) \quad (68)$$

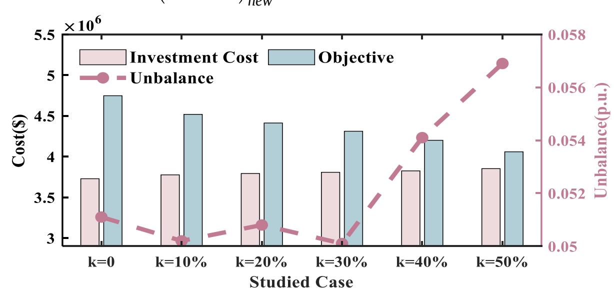

Figure 14. *Comparison results for different degradation parameters*

In Fig.14, it can be observed that as the health degradation index k increases, there is a slight rise in investment cost and a noticeable reduction in the objective value. The increasing severity of DG health degradation results in higher O&M costs for the DG units, leading to a decrease in system profits. Additionally, the capacity drop of DGs necessitates higher power purchasing costs from the utility to maintain power balance, further contributing to the decline in the objective value.

The hourly unbalance exhibits minimal changes when k is below 30%. However, once k exceeds 40%, a significant increase in hourly unbalance occurs, attributed to the severe capacity drop of DGs and the increased power exchange at the first bus in the ADNs. Hence, DG's health degradation has a significant impact on system cost estimation and three-phase unbalance, which is necessary to be modeled for a long-term planning problem to make it more applicable to real-world scenarios.

VI. CONCLUSION

This paper proposes an optimal joint planning approach for utility-owned DER units in unbalanced ADNs. The modeling of DERs asset health degradation into the problem formulation avoids the overestimation of system availability and adequacy as well as the underestimation of the system cost. Correlations of diverse uncertainties arising from the renewables and load demands are captured and the volatility of the electricity price is also well modeled. From the simulation results, the following conclusions are drawn:

(i). The linearized three-phase branch flow model enables precise decisions for installing and dispatching DERs across the three phases of unbalanced ADNs. Comparative analysis with a balanced network shows that the proposed approach effectively reduces network unbalances and enhances overall profitability.

(ii). The DERs asset health degradation model demonstrates the significant impact of asset aging on the accurate calculation of system cost and system adequacy, which affect the long-term planning results.

(iii). The copula-based two-stage SP method efficiently handles diverse uncertainties by accurately capturing correlations among dependent variables and accounting for electricity price volatility.

VII. REFERENCES

[1] D. Zhang, G. M. Shafiullah, C. K. Das, and K. W. Wong, "A systematic review of optimal planning and deployment of distributed generation and energy storage systems in power networks," *J. Energy Storage*, vol. 56, no. PA, p. 105937, 2022.

[2] Z. Wang, J. Wang, and C. Chen, "A Three-Phase Microgrid Restoration Model Considering Unbalanced Operation of Distributed Generation," *IEEE Trans. Smart Grid*, vol. 9, no. 4, pp. 3594–3604, 2018.

[3] B. Wang, C. Zhang, Z. Y. Dong, and X. Li, "Improving Hosting Capacity of Unbalanced Distribution Networks via Robust Allocation of Battery Energy Storage Systems," *IEEE Trans. Power Syst.*, vol. 36, no. 3, pp. 2174–2185, 2021.

[4] E. Samani and F. Aminifar, "Tri-Level Robust Investment Planning of DERs in Distribution Networks with AC Constraints," *IEEE Trans. Power Syst.*, vol. 34, no. 5, pp. 3749–3757, 2019.

[5] J.-H. Teng, "A direct approach for distribution system load flow solutions," *IEEE Trans. power Deliv.*, vol. 18, no. 3, pp. 882–887, 2003.

[6] M. Farivar and S. H. Low, "Branch flow model: Relaxations and convexification-part i," *IEEE Trans. Power Syst.*, vol. 28, no. 3, pp. 2554–2564, 2013.

[7] L. Gan and S. H. Low, "Convex relaxations and linear approximation for optimal power flow in multiphase radial networks," *Proc. - 2014 Power Syst. Comput. Conf. PSCC 2014*, pp. 1–9, 2014.

[8] Y. Zheng, Z. Y. Dong, K. Meng, H. Yang, M. Lai, and K. P. Wong, "Multi-objective distributed wind generation planning in an unbalanced distribution system," *CSEE J. power energy Syst.*, vol. 3, no. 2, pp. 186–195, 2017.

[9] X. Chen, W. Wu, and B. Zhang, "Robust Capacity Assessment of Distributed Generation in Unbalanced Distribution Networks Incorporating ANM Techniques," *IEEE Trans. Sustain. Energy*, vol. 9, no. 2, pp. 651–663, 2018.

[10] S. Roy Ghatak, S. Sannigrahi, and P. Acharjee, "Multiobjective Framework for Optimal Integration of Solar Energy Source in Three-Phase Unbalanced Distribution Network," *IEEE Trans. Ind. Appl.*, vol. 56, no. 3, pp. 3068–3078, 2020.

[11] X. Jia, C. Jin, M. Buzza, W. Wang, and J. Lee, "Wind turbine performance degradation assessment based on a novel similarity metric for machine performance curves," *Renew. Energy*, vol. 99, pp. 1191–1201, 2016.

[12] A. Charki, "Accelerated degradation testing of a photovoltaic module," *J. Photonics Energy*, vol. 3, no. 1, p. 033099, 2013.

[13] H. Mo and G. Sansavini, "Impact of aging and performance degradation on the operational costs of distributed generation systems," *Renew. Energy*, vol. 143, pp. 426–439, 2019.

[14] R. Ahmadi, "An optimal replacement policy for complex multi-component systems," *Int. J. Prod. Res.*, vol. 54, no. 17, pp. 5303–5316, 2016.

[15] D. Shin and K. Ko, "Comparative analysis of degradation rates for inland and seaside wind turbines in compliance with the International Electrotechnical Commission standard," *Energy*, vol. 118, pp. 1180–1186, 2017.

[16] Y. Zhang, Y. Xu, H. Yang, Z. Y. Dong, and R. Zhang, "Optimal Whole-Life-Cycle Planning of Battery Energy Storage for Multi-Functional Services in Power Systems," *IEEE Trans. Sustain. Energy*, vol. 11, no. 4, pp. 2077–2086, 2020.

[17] M. Petrelli, D. Fioriti, A. Berizzi, and D. Poli, "Multi-Year Planning of a Rural Microgrid Considering Storage Degradation," *IEEE Trans. Power Syst.*, vol. 36, no. 2, pp. 1459–1469, 2021.

[18] T. Ding, M. Qu, C. Huang, Z. Wang, P. Du, and M. Shahidehpour, "Multi-Period Active Distribution Network Planning Using Multi-Stage Stochastic Programming and Nested Decomposition by SDDIP," *IEEE Trans. Power Syst.*, vol. 36, no. 3, pp. 2281–2292, 2021.

[19] Z. Li, Y. Xu, S. Fang, and S. Mazzoni, "Optimal placement of heterogeneous distributed generators in a grid-connected multi-energy microgrid under uncertainties," *IET Renew. Power Gener.*, vol. 13, no. 14, pp. 2623–2633, 2019.

[20] D. Yu and N. Ghadimi, "Reliability constraint stochastic UC by considering the correlation of random variables with Copula theory," *IET Renew. Power Gener.*, vol. 13, no. 14, pp. 2587–2593, 2019.

[21] Y. Chi, Y. Xu, and R. Zhang, "Candidate bus selection for dynamic VAR planning towards voltage stability enhancement considering copula-based correlation of wind and load uncertainties," *IET Gener. Transm. Distrib.*, vol. 15, no. 4, pp. 780–791, 2021.

[22] A. Rezaee Jordehi, "Allocation of distributed generation units in electric power systems: A review," *Renew. Sustain. Energy Rev.*, vol. 56, pp. 893–905, 2016.

[23] Z. Li, Y. Xu, X. Feng, and Q. Wu, "Optimal stochastic deployment of heterogeneous energy storage in a residential multienergy microgrid with demand-side management," *IEEE Trans. Ind. Informatics*, vol. 17, no. 2, pp. 991–1004, 2020.

[24] "Renewable energy integration demonstrator-Singapore." https://www.ntu.edu.sg/erian/research-capabilities/renewable-energy-integration-demonstrator---singapore.

[25] Suripto and Supriyanto, "The effect of the covid-19 pandemic on stock prices with the event window approach: A case study of state gas companies, in the energy sector," *Int. J. Energy Econ. Policy*, vol. 11, no. 3, pp. 155–162, 2021

[26] Y. Wei, J. Liu, X. Lai, and Y. Hu, "Which determinant is the most informative in forecasting crude oil market volatility: Fundamental, speculation, or uncertainty?," *Energy Econ.*, vol. 68, pp. 141–150, 2017.

[27] "Open Power System Data platform." https://data.open-power-system-data.org/.

[28] B. Iooss and P. Lema\^\itre, "A review on global sensitivity analysis methods," *Uncertain. Manag. simulation-optimization complex Syst.*, pp. 101–122, 2015.

[29] G. K. Sakki, I. Tsoukalas, P. Kossieris, C. Makropoulos, and A. Efstratiadis, "Stochastic simulation-optimization framework for the design and assessment of renewable energy systems under uncertainty," *Renew. Sustain. Energy Rev.*, vol. 168, no. September, p. 112886, 2022.

[30] L. Yu, Y. P. Li, G. H. Huang, Y. R. Fan, and S. Nie, "A copula-based flexible-stochastic programming method for planning regional energy system under multiple uncertainties: A case study of the urban agglomeration of Beijing and Tianjin," *Appl. Energy*, vol. 210, no. October 2017, pp. 60–74, 2018.

[31] W. H. Kersting, "Radial distribution test feeders," *IEEE Trans. Power Syst.*, vol. 6, no. 3, pp. 975–985, 1991.

[32] "IEEE 34 Node Test Feeder." https://cmte.ieee.org/pes-testfeeders/resources/.
[33] "NREL Data Catalog." https://data.nrel.gov/submissions/126.
[34] "NREL:Grid Modernization." https://www.nrel.gov/grid/solar-power-data.html.
[35] H. Hedayati, S. A. Nabaviniaki, and A. Akbarimajd, "A method for placement of DG units in distribution networks," *IEEE Trans. power Deliv.*, vol. 23, no. 3, pp. 1620–1628, 2008.

Ruoxuan Leng (S'21) received the B.E. degree in Electrical and Electronic Engineering from both University of Edinburgh, Scotland, UK and North China Electric Power University, Beijing, China in 2020. She is currently a Ph.D. Student in School of Electrical and Electronic Engineering, Nanyang Technological University, Singapore. Her research interests include operation and planning optimization of distributed energy resources.

Zhengmao Li (S'17-M'21) received a Ph.D. degree in electrical engineering from the School of Electrical and Electronic Engineering, Nanyang Technological University, Singapore, in 2020. From 2020 to 2021, he was a Research Fellow with the Stevens Institute of Technology, Hoboken, NJ, USA. From 2021-2023, he was a research fellow at Singapore-ETH center. From April 2023, he is an assistant professor at Aalto University, Finland. His research interests include green hydrogen-based multi-energy systems, optimization, and machine learning techniques, and system resilience.

Yan Xu (S'10-M'13-SM'19) received the B.E. and M.E degrees from South China University of Technology, Guangzhou, China in 2008 and 2011, respectively, and the Ph.D. degree from The University of Newcastle, Australia, in 2013. He conducted postdoctoral research with the University of Sydney Postdoctoral Fellowship, and then joined Nanyang Technological University (NTU) with The Nanyang Assistant Professorship. He is now an Associate Professor and Deputy Director of Center for Power Engineering (CPE) at School of Electrical and Electronic Engineering, as well as a Cluster Director at Energy Research Institute @ NTU (ERI@N). His research interests include power system stability and control, microgrid, and data-analytics for smart grid applications. Dr Xu is now an Editor for IEEE Trans. Smart Grid and IEEE Trans. Power Systems and was the Chairman of the IEEE Power & Energy Society Singapore Chapter (2021 and 2022), and General Co-Chair of 11th IEEE ISGT-Asia Conference in 2022.